Unbound states in ^{17}C and p-sd shell-model interactions

S. Kim [a,b,*], J.W. Hwang [a,b], Y. Satou [b,c], N.A. Orr [d], T. Nakamura [e], Y. Kondo [e], J. Gibelin [d], N.L. Achouri [d], T. Aumann [f,g], H. Baba [h], F. Delaunay [d], P. Doornenbal [h], N. Fukuda [h], N. Inabe [h], T. Isobe [h], D. Kameda [h], D. Kanno [e], N. Kobayashi [e], T. Kobayashi [i], T. Kubo [h], S. Leblond [d], J. Lee [h,1], F.M. Marqués [d], R. Minakata [e], T. Motobayashi [h], D. Murai [j], T. Murakami [k], K. Muto [i], T. Nakashima [e], N. Nakatsuka [k], A. Navin [l], S. Nishi [e], S. Ogoshi [e], H. Otsu [h], H. Sato [h], Y. Shimizu [h], H. Suzuki [h], K. Takahashi [i], H. Takeda [h], S. Takeuchi [h], R. Tanaka [e], Y. Togano [g], A.G. Tuff [m], M. Vandebrouck [n], K. Yoneda [h]

[a] *Center for Exotic Nuclear Studies, Institute for Basic Science, Daejeon 34126, Republic of Korea*
[b] *Department of Physics and Astronomy, Seoul National University, 1 Gwanak-ro, Gwanak-gu, Seoul 08826, Republic of Korea*
[c] *Rare Isotope Science Project, Institute for Basic Science, 1 Gukjegwahak-ro, Yuseong-gu, Daejeon 34000, Republic of Korea*
[d] *LPC Caen, Normandie Université, ENSICAEN, UNICAEN, CNRS/IN2P3, F-14050 Caen, France*
[e] *Department of Physics, Tokyo Institute of Technology, 2-12-1 O-Okayama, Meguro, Tokyo 152-8551, Japan*
[f] *Institut für Kernphysik, Technische Universität Darmstadt, D-64289 Darmstadt, Germany*
[g] *ExtreMe Matter Institute EMMI and Research Division, GSI Helmholtzzentrum für Schwerionenforschung GmbH, D-64291 Darmstadt, Germany*
[h] *RIKEN Nishina Center, Hirosawa 2-1, Wako, Saitama 351-0198, Japan*
[i] *Department of Physics, Tohoku University, Aoba, Sendai, Miyagi 980-8578, Japan*
[j] *Department of Physics, Rikkyo University, 3 Nishi-Ikebukuro, Toshima, Tokyo 171-8501, Japan*
[k] *Department of Physics, Kyoto University, Kyoto 606-8502, Japan*
[l] *GANIL, CEA/DRF-CNRS/IN2P3, F-14076 Caen Cedex 5, France*
[m] *Department of Physics, University of York, Heslington, York YO10 5DD, United Kingdom*
[n] *Institut de Physique Nucléaire, Université Paris-Sud, IN2P3/CNRS, 91406 Orsay, France*

ARTICLE INFO

ABSTRACT

Unbound states in ^{17}C were investigated via one-neutron removal from a ^{18}C beam at an energy of 245 MeV/nucleon on a carbon target. The energy spectrum of ^{17}C, above the single-neutron decay threshold, was reconstructed using invariant mass spectroscopy from the measured momenta of the ^{16}C fragment and neutron, and was found to exhibit resonances at E_r=0.52(2), 0.77(2), 1.36(1), 1.91(1), 2.22(3) and 3.20(1) MeV. The resonance at E_r=0.77(2) MeV [E_x=1.51(3) MeV] was provisionally assigned as the second $5/2^+$ state. The two resonances at E_r=1.91(1) and 3.20(1) MeV [E_x=2.65(2) and 3.94(2) MeV] were identified, through comparison of the energies, cross sections and momentum distributions with shell-model and eikonal reaction calculations, as p-shell hole states with spin-parities $1/2_1^-$ and $3/2_2^-$, respectively. A detailed comparison was made with the results obtained using a range of shell-model interactions. The YSOX shell-model Hamiltonian, the cross-shell part of which is based on the monopole-based universal interaction, was found to provide a very good description of the present results and those for the neighbouring odd-A carbon isotopes – in particular for the negative parity cross-shell states.

© 2022 The Author(s). Published by Elsevier B.V. This is an open access article under the CC BY license (http://creativecommons.org/licenses/by/4.0/). Funded by SCOAP^3.

Studies of nuclei away from β stability have revealed that shell structure evolves as a function of the neutron (N) and proton (Z) asymmetry. Importantly, shell evolution is not only characterized by the appearance of new magic numbers and the disappearance of conventional ones, but also by a variety of other features [1,2]. Here the focus is placed on the lowest-lying cross-shell states in the neutron-rich isotopes of carbon. In particular, by providing improved spectroscopic information on ^{17}C, the location of these negative parity states is investigated in the light of specific components of shell-model effective interactions. Such levels have to date been the subject of a relatively limited range of studies (see,

---

for example, Refs. [3–7]). Such states are formed by the creation of a hole in the p-shell orbitals – $0\nu p_{1/2}$ or $0\nu p_{3/2}$ – and their energies depend on the interplay between: (1) the valence proton and neutron $T=0$ interaction, (2) the valence neutron-neutron interaction and (3) the valence neutron-hole interaction. As such, the energy of these states, in particular across a range of isotopes, enables elements of the shell-model effective interaction, which are not generally probed, to be explored.

In more general terms the neutron-rich carbon isotopes are of significant interest as they form part of an isotopic chain that is experimentally accessible from the proton (^{9}C) to the neutron (^{22}C) driplines. Moreover they exhibit many of the phenomena exhibited by light nuclear systems, ranging, for example, from single [8–14] and two-neutron haloes [14,15] to large deformations [16,17] and retarded electromagnetic transition rates of excited states [18–22]. In parallel, effects such as those associated with the two-body interaction have been studied [23,24] owing to the relatively large magnitude of the residual interaction. In a more fundamental vein, *ab-initio* structure calculations have also been applied to describe the neutron-rich carbon isotopes [25–28].

Focusing on the energies of the first 2^+ levels of the even-even neutron-rich carbon isotopes, it has become clear that the vacancy (of two protons) in the proton p shell below the $Z=8$ shell closure leaves traces on the shell structure and inter-nucleon interaction for the valence neutrons. First, the 2_1^+ energies for ^{16,18,20}C are very similar and quite low, which has been interpreted as the disappearance of the $N=14$ sub-shell gap in carbon [29], in contrast to the oxygen isotopes where the energy of the 2_1^+ state rises markedly at ^{22}O [30]. This is believed to be caused by the near degeneracy of the $\nu s_{1/2}$ and $\nu d_{5/2}$ orbits [29] in the carbon isotopes, as confirmed by a recent single-neutron transfer reaction study of ^{17}C [31]. Second, the conventional shell model utilizing, for example, the well established WBT interaction [32] does not reproduce the 2_1^+ energies for ^{16,18,20}C – the calculated energies are ~ 0.6 MeV higher than experiment [29,33]. Agreement can be obtained by reducing the neutron-neutron two-body matrix elements (MEs) in the sd shell by 25% (WBT* [29]), an effect which may arise from the loosely bound nature of the valence neutrons and/or the effect of core polarization [34]. In this context, improved spectroscopy of neighbouring odd-A neutron-rich carbon isotopes is likely to be useful.

Measurements of the magnetic dipole ($M1$) transition strengths from the $1/2^+$ (212 keV) and $5/2^+$ (333 keV) excited states in ^{17}C to the $3/2^+$ ground state have revealed an anomalously retarded value for $B(M1 : 1/2^+ \to 3/2^+)$, as compared to $B(M1 : 5/2^+ \to 3/2^+)$ [20,27]. This has been explained [35] by an enhancement in the tensor force in the p-sd cross-shell interaction in the SFO Hamiltonian [36] – specifically by replacing the relevant MEs of SFO with those of the $\pi + \rho$ meson exchange tensor interaction of Ref. [37]. We note that the more general issue of shell evolution driven by the tensor force was initially explored through systematic analyses of the effects of the monopole MEs [2]. In this context, the YSOX shell-model interaction [38] has been developed using parameters from the SFO (p shell), SDPF-M [39] (sd shell) and the monopole-based universal interaction V_{MU} [40] (p-sd cross shell) that contains the central, $\pi + \rho$ tensor and spin-orbit force components. The YSOX interaction has consequently been able to explain a variety of properties of light neutron-rich nuclei, including the location of the neutron drip line [38].

The present study aimed at investigating excited states above the neutron-decay threshold in the odd-A carbon isotope ^{17}C. The high-energy single-neutron removal or "knockout" from a secondary ^{18}C beam was employed in order to populate single-particle states above the one-neutron separation energy, including the p-shell hole states – spin-parity $J^\pi = 1/2^-$ and $3/2^-$ – candidates for which have been reported in a study of the β-delayed

neutron emission from ^{17}B [5]. Employing high-energy neutron knockout provides, through the reconstructed momentum distribution of the ^{17}C* beam-like residue, a means to determine directly the orbital angular momentum of the removed neutron and thus the parity of the state populated. Furthermore, this approach allows spectroscopic factors to be deduced which provide for a much more stringent test of shell-model interactions than from the energies alone. The results obtained, combined with earlier work, including that on the neighbouring odd-A isotopes ^{15,19}C, have been used to test a range of shell-model Hamiltonians.

The secondary beam of ^{18}C was produced using the BigRIPS fragment separator [41] at the RIKEN–RIBF laboratory [42]. A primary ^{48}Ca beam at 345 MeV/nucleon, and intensity of $\sim$80 pnA was used to bombard a 30-mm-thick beryllium production target. The ^{18}C ions were transported to the SAMURAI facility [43] which was employed to undertake the measurements. The energy of the ^{18}C beam at the mid-point of the secondary carbon reaction target (1.8 g/cm^2 thick) was 245 MeV/nucleon, with a momentum spread of $|\Delta p|/p \leq 3\%$. The intensity of the ^{18}C beam was around 2.3×10^3 particles per second. Particle-identification of the beam ions was determined from the magnetic rigidity ($B\rho$) (derived from a position measurement at a dispersive focal plane of BigRIPS) together with the time-of-flight (TOF) and the energy loss (ΔE) measured using an ion chamber. The trajectory of the secondary beam onto the reaction target was deduced using two position sensitive drift chambers. The beam velocity charged reaction products were momentum analysed using the large-gap (80 cm) high acceptance superconducting dipole magnet of SAMURAI (central rigidity 7 Tm). The gap of the dipole was kept under vacuum using a chamber equipped with thin large-area exit windows [44] which minimized the amount of material encountered by both the fragments and neutrons. The trajectories of the charged fragments were determined using two drift chambers – one placed at the entrance and another at the exit of the dipole. A 16-element plastic hodoscope, placed after the second drift chamber, provided measurements of the ΔE and TOF with respect to a thin plastic start detector.

The beam velocity neutrons, emitted at forward angles, were detected using the multi-element NEBULA plastic scintillator array [45,46] placed $\sim$11 m downstream of the reaction target. The array, which consisted of 120 neutron individual modules ($12 \times 12 \times 180$ cm^3) and 24 charged particle veto modules, each with a thickness of 1 cm, was configured in two walls, each composed of two layers of 30 modules. The NEBULA intrinsic detection efficiency of $31.6 \pm 1.6\%$ (for a 6 MeVee threshold setting) was derived from the measurement of quasi mono-energetic neutrons produced using the ^{7}Li$(p,n)^7$Be(g.s.+0.43 MeV) reaction at a proton energy of 250 MeV.

The de-excitation γ rays emitted from bound states of the charged fragments were detected using the DALI2 array which consisted of 140 NaI(Tl) scintillator detectors surrounding the target [47,48]. The array had a detection efficiency of 16(1)% at 1 MeV with a resolution of 150 keV (FWHM) after add-back analysis and Doppler correction.

The invariant mass method was used to reconstruct the energy above the neutron-decay threshold in ^{17}C*. Specifically, the momentum vectors of the decay products, $(E_f, \boldsymbol{p}_f)$ and $(E_n, \boldsymbol{p}_n)$ for the fragment and neutron, respectively, were used to calculate the relative energy (E_{rel}),

$$E_{rel} = \sqrt{(E_f + E_n)^2 - |\boldsymbol{p}_f + \boldsymbol{p}_n|^2} - (M_f + M_n). \qquad (1)$$

Here $M_f(M_n)$ is the mass of the fragment (neutron). The excitation energy, E_x, is related to E_{rel} as $E_x = E_{rel} + S_n (+E_\gamma)$, where S_n is the one-neutron separation energy [$S_n = 0.735(18)$ MeV for ^{17}C [49]] and E_γ is the energy of γ rays emitted from the bound excited states of ^{16}C, if populated.

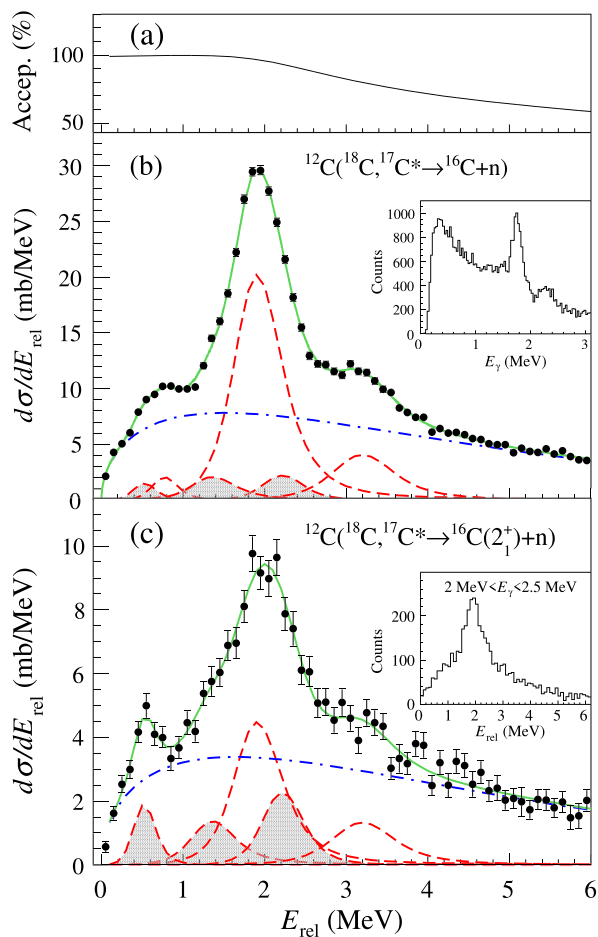**Fig. 1.** (a) The geometrical acceptance of NEBULA for one-neutron detection in co-incidence with ^{16}C for the $^{12}C(^{18}C, ^{17}C^*)$ reaction at 245 MeV/nucleon. (b) Relative energy spectrum of ^{17}C reconstructed from the measured momenta of ^{16}C and a neutron. (c) Relative energy spectrum obtained by requiring coincidence detection of the 1.77-MeV γ ray from $^{16}C(2_1^+)$. The green solid lines represent the overall fit, the red dashed lines individual resonances (the shaded peaks are those determined to be in coincidence with $^{16}C(2_1^+)$) and the blue dot-dashed lines the non-resonant continuum. The inset in (b) displays the γ-ray energy spectrum and that in (c) the relative energy spectrum (non-acceptance corrected) obtained by gating on the ~2.3 MeV structure in the γ-ray spectrum.

In order to interpret the reconstructed E_{rel} spectra a Monte Carlo simulation was developed which took into account the geometry of the setup and detectors and their resolutions as well as the beam characteristics and target effects and the reaction itself (most notably through the momentum imparted to $^{17}C^*$ under the assumption of sudden removal of a neutron, which is subject to the Fermi motion, from the ^{18}C beam). The geometrical acceptance as a function of E_{rel} is shown in Fig. 1 (a). The resolution in E_{rel} was determined to scale as $\Delta E_{rel} \approx 0.4\sqrt{E_{rel}}$ MeV (FWHM). As expected the primary effect on the resolution was the neutron detection (position and TOF). In order to obtain the final fits (see below) to describe the E_{rel} spectra, the lineshapes of the different features (resonances and non-resonant continuum) were used as input for the simulations and the various parameters (resonance energies, widths, relative weights) were varied.

The reconstructed E_{rel} spectrum, obtained from the measured ^{16}C and neutron coincidences, is displayed in Fig. 1 (b) and is dominated by a clear resonance-like peak at 2 MeV straddled by two less prominent features at around 0.7 and 3.2 MeV along with a very broad underlying distribution. The inset of panel (b) shows the coincident γ-ray spectrum which exhibits a strong peak from the well known 1.766(10)-MeV transition arising from the

de-excitation of the ^{16}C 2_1^+ state [50]. At slightly higher energy ($E_\gamma \sim 2.3$ MeV) a much weaker and somewhat broader feature appears, which arises from the decay of some or all of the members of a triplet of levels located at around 4.1-MeV excitation energy [12,50]. We note that owing to the weakness of these transitions it was not possible to clearly associate them with any of the neutron decays observed here. The spectra of panels (b) and (c) were obtained after subtracting away the contributions arising from reactions on materials other than the secondary target using data acquired with the target removed.

The spectrum displayed in Fig. 1 (c) shows the E_{rel} spectrum when requiring a coincidence with the photopeak of the 1.77-MeV transition. Whilst having a similar overall form to (b), this spectrum differs in its details. Most notably, a clear relatively narrow peak appears at $E_{rel} \sim 0.5$ MeV, which, in order to describe the broad feature at around 0.7 MeV in the inclusive spectrum, requires a γ-ray non-coincident strength at $E_{rel} \sim 0.8$ MeV [Fig. 1 (b)] to also be present. The peak at $E_{rel} \sim 1.9$ MeV in Fig. 1 (c) is not only reduced in intensity but also exhibits an asymmetric form with a width broader than in the inclusive spectrum Fig. 1 (b) and requires the inclusion of γ-ray coincident strengths at $E_{rel} \sim 1.4$ and 2.2 MeV.

The E_{rel} spectra were fitted employing R-matrix [51] line shapes with widths dependent on the decay energy and ℓ-value of the neutron decay [17] and a very broad underlying non-resonant continuum. The resonance energies (E_r), widths (Γ) and normalizations were determined using an iterative fitting procedure applied to the inclusive [Fig. 1 (b)] and the γ-ray coincidence [Fig. 1 (c)] spectra, until good convergence was achieved in describing both. Here, the fit of the inclusive spectrum proceeded with six resonances, while the γ-ray coincidence spectrum was fitted by five resonances without the resonance at $E_{rel} \sim 0.8$ MeV, which presented too small an intensity to be included. The non-resonant continuum was modelled using, as in earlier studies (e.g., Ref. [17]), a distribution with the form, $a\sqrt{E_{rel}} \exp(-bE_{rel})$, with a and b taken to be fitting parameters.

As the γ-ray spectrum exhibits a significant background, the analysis took into account such components, including, for example, the Compton scattering arising from the ~2.3-MeV γ rays, that were expected to be included when gating on the 1.77-MeV photopeak. Of the six resonances, those at E_r=0.52, 1.36 and 2.22 MeV could be clearly determined to be in coincidence with the 1.77-MeV γ ray (shaded peaks in Fig. 1). The peaks at E_r=1.91 and 3.20 MeV were determined not to be in coincidence with the 1.77-MeV γ ray. Even though they appear in Fig. 1 (c), their counting rates were ~3-4 times smaller than those expected on the basis of the spectrum of Fig. 1 (b) given the NaI(Tl) array's detection efficiency and the corresponding peaks thus arise from coincidences with background γ rays.

The resonance parameters (E_r and Γ) for the 6 different neutron-decay transitions identified here, together with the associated partial cross sections (σ_{-1n}^{exp}), are summarized in Table 1. The E_x for the E_r=1.36 and 2.22-MeV resonances are not listed since, as described below, they could not be unambiguously placed in the level scheme. The uncertainties quoted in the Table are those obtained by combining in quadrature the statistical and systematic contributions. The latter arises from the exact form of the non-resonant continuum, the neutron detection efficiency and the geometrical acceptance correction. Specifically for σ_{-1n}^{exp}, the errors resulting from statistical uncertainties are 14%, 12%, 12%, 2%, 14% and 5% for the E_r=0.52, 0.77, 1.36, 1.91, 2.22 and 3.20-MeV resonances, respectively, while those from the systematic uncertainties for the same levels are 25%, 18%, 42%, 6%, 35% and 19% arising from the choice of the non-resonant continuum, 5% (for all) from the neutron detection efficiency, and 2% (for all) from the geomet-

Table 1

Experimentally determined resonance energy (E_r), excitation energy (E_x) and width (Γ) of the unbound states in ^{17}C produced via single-neutron removal from ^{18}C in comparison with reaction and shell-model (YSOX [38]) calculations. The theoretical excitation energy (E_x^{th}) is given with respect to the $3/2_1^+$ state.

E_r (MeV)	E_x (MeV)	Γ (MeV)	ℓ ($\hbar$)	σ_{-1n}^{exp} (mb)	σ_{sp} (mb)[a,b]	C^2S^{exp} [a]	C^2S^{th}	E_x^{th} (MeV)	J^π
0.77(2)	1.51(3)	$\ll$ 0.36[c]		0.87(24)	21.93	0.035(12)	0.015	1.60	$(5/2_2^+)$
1.91(1)	2.65(2)	0.23(3)	1	17.69(75)	20.26	0.82(14)	1.350	2.53	$1/2_1^-$
0.52(2)[d]	3.02(4)	$\ll$ 0.29[c]		0.55(21)					
3.20(1)	3.94(2)	0.32(9)	1	4.61(50)[e]	19.40	0.22(4)[e]	0.174	4.18	$3/2_1^-$
1.36(1)[d]		0.27(13)		1.73(44)[e]					
2.22(3)[d]		< 0.05		1.50(39)					

[a] An uncertainty of $\pm15\%$ associated with the reaction modeling is estimated for σ_{sp} and is included in the uncertainty in C^2S^{exp} (see text).

[b] S_n^{eff} derived from E_x were used in the reaction calculations.

[c] Upper limit corresponding to the experimental resolution at the corresponding relative energy.

[d] Observed in coincidence with ^{16}C(2_1^+) de-excitation γ rays.

[e] If the E_r=1.36-MeV transition is a decay branch of the $3/2_1^-$ level to ^{16}C(2_1^+), the total cross section to the $3/2_1^-$ state is 6.34(67) mb and C^2S^{exp}=0.31(6) (see text).

rical acceptance correction. The errors in E_r and Γ were dominated by the statistical uncertainties.

Turning now to the spectroscopic factors, the single-neutron removal cross section σ_{-1n} can be expressed in a factorized form as [52],

$$\sigma_{-1n} = \sum_{n\ell j} \left(\frac{A}{A-1}\right)^N C^2S(J^\pi, n\ell j)\sigma_{sp}(n\ell j, S_n^{eff}), \quad (2)$$

where $n\ell j$ refers to the quantum numbers of the removed neutron, C^2S the spectroscopic factor, σ_{sp} the single-particle cross section, $[A/(A-1)]^N$ the center-of-mass correction factor [53] with A the mass number of the projectile and N the major oscillator quantum number (N=2n+ℓ), and S_n^{eff} the effective single-neutron separation energy given by the sum of S_n of the projectile [S_n(^{18}C)=4.18(4) MeV [49]] and E_x of the state in ^{17}C*.

Shell-model spectroscopic factors (C^2S^{th}) and excitation energies (E_x^{th}) were computed using the NUSHELLX@MSU code [54] and the YSOX interaction [38] in the p-sd model space (Table 1). No explicit restriction in terms of the $\hbar\omega$ excitations was applied. The shell-model spectroscopy for positive (negative) parity states is compared with experimental data available for ^{17}C in Fig. 2 (Fig. 3), where the calculations are supplemented by the results obtained using the WBT [32], WBT* [29] and *ab initio* Coupled-Cluster Effective Interaction (CCEI) [26] (for positive parity states only) interactions. The calculations utilizing the WBT and WBT* interactions were performed using the OXBASH code [55] in the s-p-sd-pf model space for $0\hbar\omega$ ($1\hbar\omega$) excitations for the positive (negative) parity states.

The σ_{sp} was computed using MOMDIS [56]. The single-particle wave function was calculated using a Wood-Saxon potential whose geometry is constrained to Hartree-Fock (HF) results using the SkX interaction [57] as described in Ref. [58]. The range parameter of the nucleon-nucleon profile function [59] was fixed at zero for the present energy of 245 MeV/nucleon [52]. The nucleon density distribution of the ^{17}C core was estimated using a HF calculation using the SkX interaction [57]. The density distribution of the carbon target was chosen to be of a Gaussian form with a point nucleon rms radius of 2.32 fm. An overall uncertainty of $\pm15\%$ (included in the uncertainties assigned to the C^2S^{exp} in Table 1) was estimated for σ_{sp}, which arises from uncertainties in the size of the unbound core ($\pm10\%$) and in the reaction theory ($\pm10\%$) [13,60]. The computed σ_{sp} and associated C^2S^{exp}, deduced from σ_{-1n}^{exp} using Eq. (2), for the relevant states are tabulated in Table 1.

Longitudinal momentum distributions for the ^{17}C* knock-out residues populating the resonances observed at E_r=1.91 and 3.20 MeV [E_x=2.65(2) and 3.94(2) MeV] were deduced, and the results are shown in Fig. 4. We note that for the other less strongly
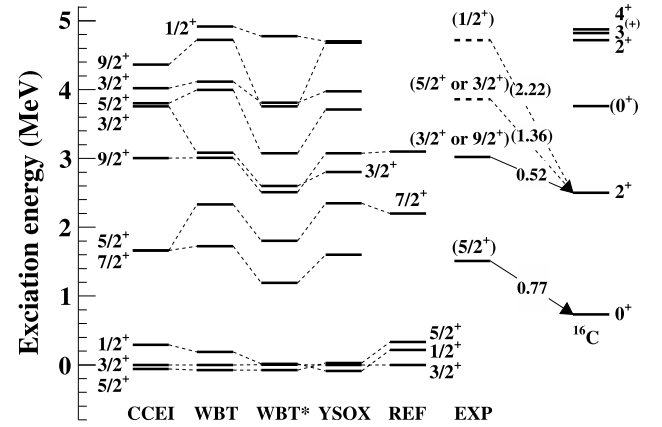

Fig. 2. Excitation energies of low-lying positive parity states of ^{17}C. The energies calculated with the shell model using the CCEI [26], WBT [32], WBT* [29] and YSOX [38] interactions are compared with those of previously observed levels (REF) [4,17,27] and the present results (EXP). The excitation energies for theory are measured with respect to the $3/2_1^+$ state. Neutron decays leading to bound states in ^{16}C are shown by arrows with the energy of the transition indicated in MeV. Candidate levels for the 1.36 and 2.22-MeV transitions are shown by dashed lines.
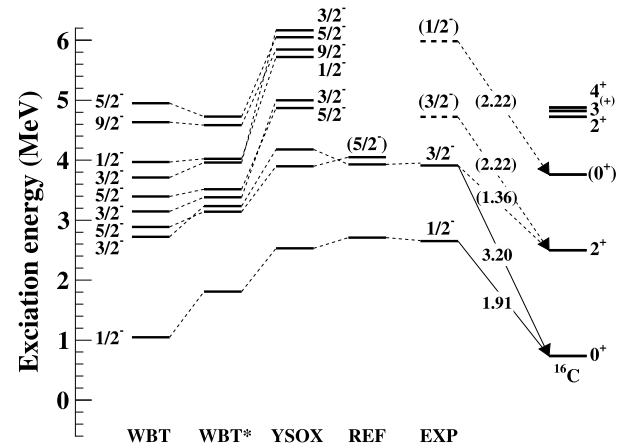

Fig. 3. Same as Fig. 2, but for negative parity states.

populated levels it was not possible to derive reliable results. In order to construct the momentum distributions, an inclusive E_{rel} spectrum was created for each bin in longitudinal momentum and was fit as described above. The error bars shown are statistical. Theoretical momentum distributions for neutron stripping, which is the dominant mechanism at the present beam energy, were calculated using the MOMDIS code for removal of a valence neutron
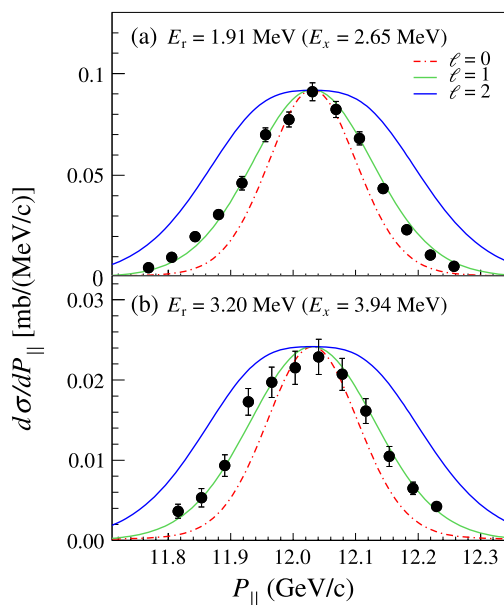
Fig. 4. Experimental longitudinal momentum distributions (filled circles) for the $^{12}C(^{18}C,\ ^{17}C^*)$ reaction for (a) the E_x=2.65-MeV and (b) 3.94-MeV states. The theoretical distributions for removal of a neutron with ℓ=0, 1 and 2 (red dot-dashed, green solid and blue solid lines, respectively) include the experimental resolution.

with angular momentum of ℓ=0, 1 and 2. In order to compare with the observed distributions, the predictions were convoluted with an experimental resolution of 31 MeV/c (sigma in the beam rest frame). As may be seen in Fig. 4 both levels are clearly associated with the removal of an ℓ=1 neutron. As such, these are negative parity states formed by a neutron hole in the p shell. Considering the hierarchy of the neutron $p_{1/2}$ and $p_{3/2}$ orbits, the former is closer to the Fermi level, and the J^π assignments of $1/2_1^-$ and $3/2_1^-$ for the E_x=2.65 and 3.94-MeV levels, respectively, are in order. These results are consistent with the β-delayed neutron-decay experiment [5] which observed the states in question at E_x=2.71(2) and 3.93(2) MeV and inferred the same assignments. As shown in Fig. 3 and in Table 1, these conclusions are in very good agreement with the shell-model calculations using the YSOX interaction. It is worthwhile noting that the use of neutron knockout, as indicated in the introduction, provided for more direct assignment. For example, a $5/2^-$ assignment (possible in the β-decay study) for the 3.93 MeV level, is impossible in the present study as there is no occupancy of the $p_{5/2}$ neutron orbital in the ^{18}C projectile.

The resonance at E_r=0.77 MeV was not found to be associated with γ-ray emission, and is thus located at E_x=1.51(3) MeV. The YSOX interaction shell-model predictions place two positive parity states, $5/2_2^+$ and $7/2_1^+$ (Fig. 2), above the single-neutron emission threshold of ^{17}C and below the $^{16}C(2_1^+)+n$ threshold of E_x=2.50 MeV. A J^π=$7/2_1^+$ assignment has been reported for a level at E_x=2.20 MeV observed in the (p, p') reaction [17]. In addition, direct single-neutron removal from ^{18}C is not expected to populate the $7/2_1^+$ state. As such the E_x=1.51-MeV state we observe here is very likely the $5/2_2^+$ level, which is predicted to lie at E_x^{th}=1.60 MeV by the YSOX calculations (Table 1). We note that an importance-truncated no-core shell-model (IT-NCSM) calculation incorporating the chiral nucleon-nucleon and three-nucleon interactions predicts the $5/2_2^+$ state at 1.78 MeV when employing the largest tractable basis size (N_{max}=6) [27]. In addition, the predicted energy difference between the $5/2_1^+$ and $5/2_2^+$ levels of 1.27 MeV is compatible with the present observation of 1.18(3) MeV.

The E_r=0.52-MeV resonance was observed in coincidence with the $^{16}C(2_1^+)$ de-excitation γ ray and exhibits the lowest decay en-

ergy of all the states observed here. Since the phase space for the two-body decay is proportional to the square root of the decay energy, such a small transition energy is very probably associated with a state which has a unique decay path. Further the E_{rel} spectrum obtained by gating on the $\sim$2.3 MeV structure in the γ-ray spectrum, which corresponds to a multiplet of states at around E_x=4.0 MeV in ^{16}C, did not exhibit any enhanced strength around E_{rel}=0.52 MeV [Fig. 1 (c) inset]. As such, the state in question is located at E_x=3.02(4) MeV. Two of the YSOX interaction shell-model levels – $3/2_2^+$ and $9/2_1^+$ – which are predicted to lie at E_x^{th} of 2.80 and 3.07 MeV, respectively, are possible candidates for this state (Fig. 2). We note that a candidate for the $9/2_1^+$ level was identified at 3.10(2) MeV in the three-neutron transfer reaction $^{14}C(^{12}C,\ ^9C)$ [4]. The decay of the $3/2_2^+$ level proceeds via s-wave neutron emission, while that of $9/2_1^+$ via d-wave neutron emission. The former is expected to result in a very broad structure, whilst the higher angular momentum of the latter would result in a rather narrow peak, as observed here, and is thus favoured. Such an assignment would imply, however, that the single-neutron knockout from ^{18}C populating this level proceeds via a multi-step process. For example, in a first step the $^{18}C(5_1^+)$ level at E_x^{th}=7.68 MeV (YSOX) might be populated by inelastic scattering and subsequently decay via s-wave neutron emission to the $^{17}C(9/2_1^+)$ state.

The remaining two peaks observed at E_r=1.36 and 2.22 MeV were populated with cross sections of the order of 1 mb, and both were observed in coincidence with the de-excitation γ ray from $^{16}C(2_1^+)$. In order to explore possible J^π assignments and locate the states in the energy level scheme of ^{17}C the properties of the single-neutron decay of low-lying shell-model (YSOX) levels have been explored through calculations of the partial decay widths and branching ratios. Although no definite conclusion could be reached, in particular because of the increased level densities at higher E_x, tentative suggestions for their possible placements are indicated in Figs. 2 and 3. It may be noted that if, as shown in Fig. 3, the E_r=1.36-MeV resonance corresponds to a decay branch of the $3/2_1^-$ state to $^{16}C(2_1^+)$, the total neutron removal cross section will be $\sigma_{-1n}^{exp}(3/2_1^-)$=6.34(67) mb with a corresponding spectroscopic factor of C^2S^{exp}=0.31(6).

Turning to the negative parity cross-shell states, Ueno et al. [5] have argued that the lower than observed energies predicted by the WBT shell-model interaction for the lowest-lying negative parity $1/2_1^-$ and $3/2_1^-$ states in ^{17}C (Fig. 3) can be remedied by reducing by 30% the diagonal pairing terms of the sd-shell MEs, $V_{J=0,T=1}$ [WBT($0.7V_{01}$)]. Here J and T refer to the angular momentum and isospin, respectively, of the corresponding two-particle state. Reduced effects of polarization of the core (carbon isotopes having two less protons in the p shell than oxygen) are the source of the diminished pairing terms in this model. This approach is examined in the following by comparing the present results and those for the neighbouring odd carbon isotopes, $^{15,19}C$, with prediction using other shell-model Hamiltonians.

Fig. 5 compares the energies with respect to the $1/2_1^+$ (^{15}C), $3/2_1^+$ (^{17}C) and $1/2_1^+$ (^{19}C) states of the (a) $1/2_1^-$ and (b) $3/2_1^-$ states in $^{15,17,19}C$ with shell-model calculations utilizing the YSOX [38] (described earlier), WBT [32], WBT($0.7V_{01}$) [5] and MK [62] interactions. A $0,2\hbar\omega$ ($1,3\hbar\omega$) basis was used for the OXBASH calculations of the positive (negative) parity states in ^{15}C. Calculations with the MK interaction were performed in the p-sd model space using the OXBASH code. As pointed out in Ref. [5], the WBT energy for $1/2_1^-$ in ^{17}C is too low by $\sim$1.5 MeV as compared to experiment [E_x=2.65(2) MeV], while the energy calculated using the WBT($0.7V_{01}$) interaction is in much better agreement. For the $1/2_1^-$ level in ^{19}C [E_x=2.89(10) MeV [7]], the WBT prediction is again too low (E_x^{th}=0.64 MeV), while the WBT($0.7V_{01}$)
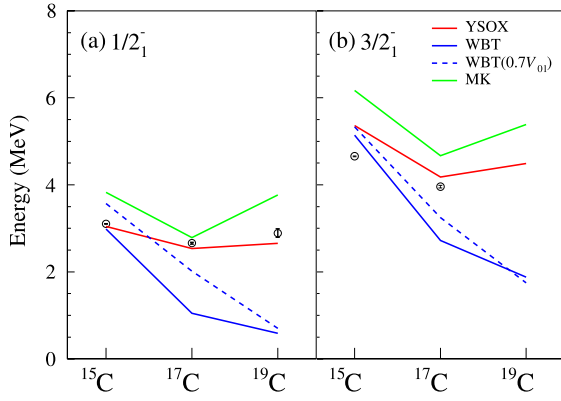
Fig. 5. Energies with respect to the $1/2^+_1$ (^{15}C), $3/2^+_1$ (^{17}C) and $1/2^+_1$ (^{19}C) states of (a) the $1/2^-_1$ and (b) $3/2^-_1$ states in ^{15,17,19}C. The experimental energies (open circles) are from the present work for ^{17}C and Refs. [7,61] for ^{15,19}C. Shell-model calculations utilizing the YSOX [38] (red solid lines), WBT [32] (blue solid lines), WBT($0.7V_{01}$) [5] (blue dashed lines) and MK [62] (green solid lines) interactions are shown for comparison (see text).

does not provide a better estimate either. This difference in the effects of reducing the diagonal pairing terms of the WBT interaction on the calculated energies of the $1/2^-_1$ states in ^{17,19}C can be understood as follows. The dominant neutron configurations for the $3/2^+_1$ ground state of ^{17}C are $\nu(d_{5/2})^3$ (seniority $v = 3$) and $\nu(d_{5/2})^2(s_{1/2})^1$ [12,38] and for the $1/2^-_1$ level $\nu(p_{1/2})^{-1}(sd)^4$. The reduced pairing has little effect on the binding of the ground state, while it makes the $1/2^-_1$ state less bound, resulting in a higher E_x. In ^{19}C, the $1/2^+_1$ ground state [8,10,12] and the $1/2^-_1$ state have primarily $\nu(s_{1/2})^1(sd)^4$ and $\nu(p_{1/2})^{-1}(sd)^6$ neutron configurations, respectively. The reduced pairing makes both of the states less bound, resulting in a limited increase ($\sim$0.11 MeV) in the calculated E_x^{th} for the $1/2^-_1$ state. It may be noted that while the WBT interaction provides a very good prediction for the energy of ^{15}C($1/2^-_1$), this agreement deteriorates for WBT($0.7V_{01}$).

The locations of the cross-shell states in ^{15,17,19}C are, as may be seen in Fig. 5, best described by the YSOX interaction predictions. Three favourable features of YSOX are worth noting in this context. First, the $\langle (d_{5/2})^2|V|(d_{5/2})^2 \rangle_{J=0,T=1}$ pairing term has already been reduced in the SDPF-M interaction [38], on which the sd part of YSOX is based. Second, the T=0 tensor force in the p-sd cross-shell part of YSOX, originating from the $\pi + \rho$ tensor force [37], is stronger than in the WBT interaction (see Fig. 2 (a) of Ref. [38]): the monopole MEs $\langle p_{1/2}d_{5/2}|V|p_{1/2}d_{5/2} \rangle^T_{T=0}$ ($\langle p_{3/2}d_{5/2}|V|p_{3/2}d_{5/2} \rangle^T_{T=0}$) are more attractive (repulsive) in YSOX. In closed p-shell nuclei, the overall contribution from these two terms is limited, while in open p-shell nuclei, their interplay plays a key role. In the neutron-rich carbon isotopes of interest here, the effect is mainly repulsive – the stronger repulsion between the $\pi p_{3/2}$ and $\nu d_{5/2}$ orbits raises the $\nu d_{5/2}$ orbit in energy, resulting in higher E_x for the cross-shell states. Third, the monopole MEs for the neutron-neutron ($T = 1$) central force, $\langle p_{1/2}d_{5/2}|V|p_{1/2}d_{5/2} \rangle^C_{T=1}$ and $\langle p_{3/2}d_{5/2}|V|p_{3/2}d_{5/2} \rangle^C_{T=1}$, are repulsive in WBT, while they are slightly attractive in YSOX (see Fig. 2 (b) of Ref. [38]). This has the following consequences when one neutron in the $\nu p_{1/2}$ or $\nu p_{3/2}$ orbit is removed. In the WBT description, the $d_{5/2}$ neutrons are subject to less repulsion from the neutrons in the p orbits, resulting in smaller predicted E_x^{th} for the hole states, while for the YSOX interaction the opposite occurs. Note that in the neutron-rich carbon isotopes, the $\nu s_{1/2}$ and $\nu d_{5/2}$ orbits are essentially degenerated [29], which leads to extensive configuration mixing owing to many-body correlations [23]. As the $\nu d_{5/2}$ orbit plays a major role in the sd-valence space, the above argument will be valid for many of the excited states.

The MK interaction [62] provides a moderately good description of the cross-shell states (Fig. 5). This interaction shares a key character with YSOX in that it incorporates non-central components – specifically the tensor force as fixed by the underlying NN interaction. This feature is believed to be primarily responsible for the inversion of the neutron $d_{5/2}$ and $s_{1/2}$ states in ^{15}C [62]. It may be noted that the MK interaction was developed to reproduce the spectroscopic features of nuclei in the mass range A=11 to 16. As shown here the extension to ^{17,19}C suggests that it performs reasonably well at somewhat higher mass number.

In terms of the positive parity states it may be seen (Fig. 2) that both the WBT and YSOX interactions predict similar energies for the $5/2^+_2$, $7/2^+_1$ and $9/2^+_1$ states, which compare well with experiment. On the other hand, the energies calculated using the WBT* interaction for these states are lower by $\sim$0.5 MeV. This is in contrast to the case of the 2^+_1 states in ^{16,18,20}C [25,29], where WBT* better describes their locations. A similar observation may be made for ^{19}C where the energy of the $5/2^+_2$ state [E_x=1.46(10) MeV [17]] is well accounted for by WBT (E_x^{th}=1.40 MeV), but not by WBT* (E_x^{th}=1.08 MeV). Sieja et al. [24] have shown that the 2^+_1 energy in ^{16}C could be satisfactorily reproduced within the shell model by introducing an asymmetric core (^{10}He) and an effective interaction which takes into account proton core polarization contributions up to third order with the inclusion of folded diagrams. This demonstrates that for asymmetric systems in which the valence spaces of protons and neutrons span two different major shells, special attention needs to be paid to the construction of the shell-model MEs. It may also be noted that the CCEI results [26] provide a consistent description of the energies for both the half-integer-spin $5/2^+$ and $9/2^+$ states in ^{17}C (Fig. 2) and the integer-spin 2^+_1 states in ^{18,20}C (see Fig. 3 of Ref. [26]). In ^{19}C the energy of the $5/2^+_2$ state with respect to the $1/2^+_1$ level (experimentally the ground state) is also well reproduced by the CCEI calculations (Fig. 4 in Ref. [7]).

In summary, the spectroscopy of neutron unbound states in ^{17}C has been investigated using single-neutron removal from ^{18}C. Resonances that were determined to lie at E_x=2.65(2) and 3.94(2) MeV were demonstrated to correspond to p-wave hole states with J^π of $1/2^-_1$ and $3/2^-_1$, respectively. Additionally, another resonance at E_x=1.51(3) MeV has been provisionally assigned J^π=$5/2^+_2$. Given that this level can provide insight into the neutron-neutron interaction in proton-neutron asymmetric systems [29] a confirmation of this assignment would be welcome. Comparison with the predictions provided by a range of shell-model interactions for levels in ^{17}C, as well as the neighbouring odd-A isotopes ^{15,19}C, demonstrated that the YSOX interaction provides the best agreement, including for the cross-shell $1/2^-_1$ and $3/2^-_1$ states.

Declaration of competing interest

The authors declare that they have no known competing financial interests or personal relationships that could have appeared to influence the work reported in this paper.

Data availability

The data that has been used is confidential.

Acknowledgements

References

[1] O. Sorlin, M.-G. Porquet, Prog. Part. Nucl. Phys. 61 (2008) 602.
[2] T. Otsuka, et al., Rev. Mod. Phys. 92 (2020) 015002.
[3] G. Raimann, et al., Phys. Rev. C 53 (1996) 453.
[4] H.G. Bohlen, et al., Eur. Phys. J. A 31 (2007) 279.
[5] H. Ueno, et al., Phys. Rev. C 87 (2013) 034316.
[6] Y. Satou, et al., Phys. Lett. B 728 (2014) 462;
    H.T. Fortune, Y. Satou, Phys. Rev. C 90 (2014) 034308.
[7] J.W. Hwang, et al., Phys. Lett. B 769 (2017) 503;
    J.W. Hwang, et al., Phys. Lett. B 774 (2017) 723.
[8] D. Bazin, et al., Phys. Rev. Lett. 74 (1995) 3569.
[9] F.M. Marqués, et al., Phys. Lett. B 381 (1996) 407.
[10] T. Nakamura, et al., Phys. Rev. Lett. 83 (1999) 1112.
[11] E. Sauvan, et al., Phys. Lett. B 491 (2000) 1.
[12] V. Maddalena, et al., Phys. Rev. C 63 (2001) 024613.
[13] E. Sauvan, et al., Phys. Rev. C 69 (2004) 044603.
[14] N. Kobayashi, et al., Phys. Rev. C 86 (2012) 054604.
[15] Y. Togano, et al., Phys. Lett. B 761 (2016) 412.
[16] H. Ogawa, et al., Eur. Phys. J. A 13 (2002) 81.
[17] Y. Satou, et al., Phys. Lett. B 660 (2008) 320.
[18] N. Imai, et al., Phys. Rev. Lett. 92 (2004) 062501.
[19] H.J. Ong, et al., Phys. Rev. C 78 (2008) 014308.
[20] D. Suzuki, et al., Phys. Lett. B 666 (2008) 222.
[21] M. Wiedeking, et al., Phys. Rev. Lett. 100 (2008) 152501.
[22] M. Petri, et al., Phys. Rev. Lett. 107 (2011) 102501.
[23] C.X. Yuan, C. Qi, F.R. Xu, Nucl. Phys. A 883 (2012) 25.
[24] K. Sieja, F. Nowacki, Nucl. Phys. A 857 (2011) 9.
[25] M. Petri, et al., Phys. Rev. C 86 (2012) 044329.
[26] G.R. Jansen, et al., Phys. Rev. Lett. 113 (2014) 142502.
[27] D. Smalley, et al., Phys. Rev. C 92 (2015) 064314.
[28] D.T. Tran, et al., Nat. Commun. 9 (2018) 1594.
[29] M. Stanoiu, et al., Phys. Rev. C 78 (2008) 034315.
[30] M. Stanoiu, et al., Phys. Rev. C 69 (2004) 034312.
[31] X. Pereira-López, et al., Phys. Lett. B 811 (2020) 135939.
[32] E.K. Warburton, B.A. Brown, Phys. Rev. C 46 (1992) 923.
[33] S. Kim, et al., AIP Conf. Proc. 1947 (2018) 020006.
[34] T.T.S. Kuo, G.E. Brown, Nucl. Phys. 85 (1966) 40.
[35] T. Suzuki, T. Otsuka, Phys. Rev. C 78 (2008) 061301(R).
[36] T. Suzuki, R. Fujimoto, T. Otsuka, Phys. Rev. C 67 (2003) 044302.
[37] T. Otsuka, et al., Phys. Rev. Lett. 95 (2005) 232502.
[38] C. Yuan, et al., Phys. Rev. C 85 (2012) 064324.
[39] Y. Utsuno, T. Otsuka, T. Mizusaki, M. Honma, Phys. Rev. C 60 (1999) 054315.
[40] T. Otsuka, et al., Phys. Rev. Lett. 104 (2010) 012501.
[41] T. Kubo, Nucl. Instrum. Methods Phys. Res., Sect. B 204 (2003) 97.
[42] Y. Yano, Nucl. Instrum. Methods Phys. Res., Sect. B 261 (2007) 1009.
[43] T. Kobayashi, et al., Nucl. Instrum. Methods Phys. Res., Sect. B 317 (2013) 294.
[44] Y. Shimizu, et al., Nucl. Instrum. Methods Phys. Res., Sect. B 317 (2013) 739.
[45] T. Nakamura, Y. Kondo, Nucl. Instrum. Methods Phys. Res., Sect. B 376 (2016) 156.
[46] Y. Kondo, T. Tonami, T. Nakamura, Nucl. Instrum. Methods Phys. Res., Sect. B 463 (2020) 173.
[47] S. Takeuchi, et al., Nucl. Instrum. Methods Phys. Res., Sect. A 763 (2014) 596.
[48] P. Doornenbal, private communication.
[49] M. Wang, et al., Chin. Phys. C 36 (2012) 1603.
[50] D.R. Tilley, H.R. Weller, C.M. Cheves, Nucl. Phys. A 564 (1993) 1.
[51] A.M. Lane, R.G. Thomas, Rev. Mod. Phys. 30 (1958) 257.
[52] P.G. Hansen, J.A. Tostevin, Annu. Rev. Nucl. Part. Sci. 53 (2003) 219.
[53] A.E.L. Dieperink, T. de Forest Jr., Phys. Rev. C 10 (1974) 543.
[54] B.A. Brown, W.D.M. Rae, Nucl. Data Sheets 120 (2014) 115.
[55] B.A. Brown, et al., MSU-NSCL report number 1289.
[56] C.A. Bertulani, A. Gade, Comput. Phys. Commun. 175 (2006) 372.
[57] B.A. Brown, Phys. Rev. C 58 (1998) 220.
[58] A. Gade, et al., Phys. Rev. C 77 (2008) 044306.
[59] L. Ray, Phys. Rev. C 20 (1979) 1857.
[60] F. Carstoiu, E. Sauvan, N.A. Orr, A. Bonaccorso, Phys. Rev. C 70 (2004) 054602.
[61] F. Ajzenberg-Selove, Nucl. Phys. A 523 (1991) 1.
[62] D.J. Millener, D. Kurath, Nucl. Phys. A 255 (1975) 315.